Y-Stabilized ZrO_2 as a Promising Wafer Material for the Epitaxial Growth of Transition Metal Dichalcogenides

*Rongbin Wang, Martin Schmidbauer, Norbert Koch, Jens Martin, and Sergey Sadofev**

Y-stabilized ZrO_2 (YSZ) as a promising single-crystal wafer material for the epitaxial growth of transition metal dichalcogenides applicable for both physical (PVD) and chemical vapor deposition (CVD) processes is used. MoS_2 layers grown on YSZ (111) exhibit sixfold symmetry and in-plane epitaxial relationship with the wafer of $(10\bar{1}0)$ MoS_2 || $(\bar{2}11)$ YSZ. The PVD-grown submonolayer thin films show nucleation of MoS_2 islands with a lateral size of up to 100 nm and a preferential alignment along the substrate step edges. The layers exhibit a strong photoluminescence yield as expected for the 2H-phase of MoS_2 in a single monolayer limit. The CVD-grown samples are composed of triangular islands of several micrometers in size in the presence of antiparallel domains. The results represent a promising route toward fabrication of wafer-scale single-crystalline transition metal dichalcogenide layers with a tunable layer thickness on commercially available wafers.

1. Introduction

Transition metal dichalcogenides (TMDCs) are considered as promising next-generation optoelectronic materials, owing to their intriguing physical properties appearing as a result of an intrinsically layered structure, specific crystal symmetry, and distinctly different optoelectronic properties of a large variety of polytypes.[1,2] To fully understand and explore the potential of TMDCs, single-crystalline wafer-scale films with tuneable material composition, layer thickness, and crystalline excellence comparable to, or even exceeding that of currently available bulk crystals, are needed. However, synthesis of the films, satisfying these requirements, remains very challenging. Despite van der Waals nature of the materials, growing them on available non-van der Waals wafers leads to a strong nuclei–wafer interaction, predefining structural imperfection of the deposited layers. The choice of suitable substrates for the epitaxial growth of TMDCs is limited not only by purely crystallographic considerations, but also wafer resistance against melting, decomposition, and chemical reactions with chalcogen atoms at elevated temperatures. These conditions are required for the most widely used fabrication techniques, including physical vapor deposition (PVD) and chemical vapor deposition (CVD). The commonly used basal plane of sapphire is thermally and chemically stable and withstands even the harsh environment of the CVD process. However, the in-plane lattice mismatch between classical TMDCs (e.g., 2H-polytype MoS_2 $a_{MoS2} = 3.161$ Å, $c_{MoS2} = 12.295$ Å[3,4]) and sapphire ($a_{Al2O3} = 4.76$ Å, $c_{Al2O3} = 13.00$ Å) is huge (about −34%). As a result of coincidental matching of several lattice units, two types of in-plane rotational domains induced by domain-match epitaxy have been reported. The first configuration corresponds to the $3 \times a_{TMDC} \approx 2 \times a_{Al2O3}$ supercell matching. The second variant involves a 30° (or 90°) rotation of the TMDC lattice with respect to sapphire and larger supercell consisting of five TMDC units ($5 \times a_{TMDC} \approx 2\sqrt{3} \times a_{Al2O3}$, R30° configuration).[5] Although the R30° configuration is expected to be most energetically favorable, both variants or even a random orientation of crystalline domains are often observed in synthetized films.[6–8] Despite the fact that the excellent device performance for the layers grown on sapphire has been successfully demonstrated,[9] there are very few reports on single-crystalline wafer-scale growth that have appeared only recently.[5,10,11] The large mismatch between MoS_2 and sapphire becomes even more severe for layers grown by PVD, where the growth temperatures are several hundred degrees lower, compared to the CVD technique. In this case, the surface diffusion of adatoms is low, and the typical domain size is in the tens-nm range.[12] Merging the individual crystallites in a quasicontinuous film without preserving long-range epitaxial registry leads to a high density of grain boundaries, negatively affecting optical and electrical properties of the layers. As a possible alternative to sapphire, we utilize cubic YSZ (111) as commonly available substrate for TMDC growth. Here, we demonstrate the suitability of YSZ for epitaxial growth of MoS_2 with pure sixfold symmetry for both PVD and CVD processes.

R. Wang, N. Koch
Institut für Physik & IRIS Adlershof
Humboldt-Universität zu Berlin
12489 Berlin, Germany

M. Schmidbauer, J. Martin, S. Sadofev
Leibniz-Institut für Kristallzüchtung
12489 Berlin, Germany
E-mail: sergey.sadofiev@ikz-berlin.de

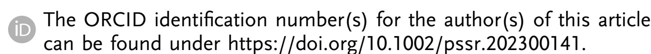
The ORCID identification number(s) for the author(s) of this article can be found under https://doi.org/10.1002/pssr.202300141.

© 2023 The Authors. physica status solidi (RRL) Rapid Research Letters published by Wiley-VCH GmbH. This is an open access article under the terms of the Creative Commons Attribution License, which permits use, distribution and reproduction in any medium, provided the original work is properly cited.

DOI: 10.1002/pssr.202300141

© 2023 The Authors. physica status solidi (RRL) Rapid Research Letters published by Wiley-VCH GmbH

2. Results and Discussion

ZrO_2 can be stabilized by Y as a face-centered-cubic fluorite structure with a lattice parameter depending on the Y-molar fraction. The material is generally known as a substrate for In_2O_3-based bixbyite compounds.[13] A closely packed YSZ (111) cubic substrate ($a = 5.147$ Å, Crystec GmbH) with a nominal Y doping level of 9 mol%) exhibits an in-plane lattice spacing along the $[1\bar{1}0]$ direction of $a_{\mathrm{YSZ}\ 110} = 3.639$ Å. This coincides with the in-plane lattice parameter a_{MoS2} of 2H-MoS_2 with a lattice mismatch of about –13.1%. At first, we address the PVD growth of multilayer and single-monolayer (ML) films.

The multilayer samples were structurally characterized using high-resolution X-ray diffraction. The corresponding out-of-plane measurements (2θ–ω scan) show a prominent peak at about $2\theta = 14.0°$, which can be assigned to the MoS_2 00.2 Bragg reflection (**Figure 1**a). The resulting vertical lattice parameter of $c_{\mathrm{exp}} = 12.7$ Å is in approximate agreement with the literature value of $c_{\mathrm{MoS2}} = 12.3$ Å.[4] In the immediate vicinity of the Bragg reflection, pronounced thickness fringes are observed, indicating a rather smooth interface between the substrate and the layer. From the angular spacing of the fringes, we can determine a MoS_2 film thickness of $t = 34.8(7)$ Å, which corresponds to about five MLs. A rocking curve (ω-scan) carried out at $2\theta = 14.0°$ (Figure 1b) shows a full width at half maximum value of about $\Delta\omega = 51$ arcsec, which is close to the experimental resolution of the instrument. This shows that the MoS_2 layer was planar on the YSZ substrate. In-plane measurements under grazing incidence (GIXD) were performed to determine the full epitaxial relationship between the MoS_2 layer and the YSZ substrate. Figure 1c shows two in-plane rocking curves (ϕ-scans) taken at $2\theta = 32.9°$ (corresponding to the MoS_2 10.0 Bragg reflection) and at $2\theta = 49.7°$ (corresponding to the YSZ $2\bar{2}0$ Bragg reflection). From these curves, it is first clear that the layer and substrate exhibit sixfold in-plane symmetry. The width $\Delta\phi_{\mathrm{sub}} = 0.1°$ of the substrate reflections matches approximately the experimental angular resolution, while the layer reflections are noticeably wider ($\Delta\phi_{\mathrm{layer}} = 1.8°$). However, this in-plane mosaic spread is more than a factor of 2 smaller than for MoS_2 layers grown on sapphire ($\Delta\phi_{\mathrm{layer}} = 4.2°$), see Figure S1, Supporting Information. Besides the observed strong layer reflections, no other Bragg reflections attributable to the MoS_2 layer appear, that is, no 90° variant is observed. This underlines a clear epitaxial relation between layer and substrate. From the relative position of layer and substrate reflections, it is evident that the MoS_2 $10\bar{1}0$ net-planes are oriented parallel to the YSZ

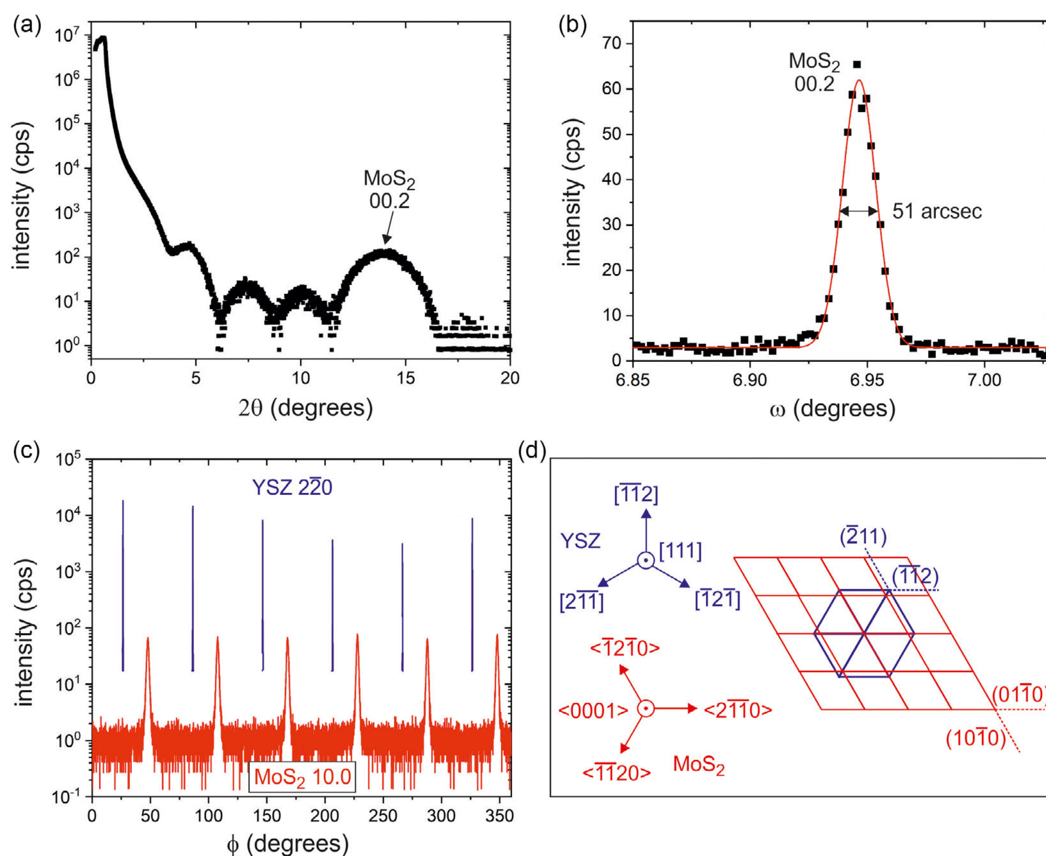

Figure 1. Structural properties of a 3.5 nm MoS_2 layer grown by PVD on YSZ (111) wafer. a) Out-of-plane X-ray diffraction 2θ–ω scan in the vicinity of the MoS_2 00.2 Bragg reflection. b) Corresponding experimental X-ray rocking curve (ω scan) at the MoS_2 00.2 Bragg reflection fit with a Gaussian line profile (red line). c) GIXD in-plane X-ray diffraction rocking curves (ϕ-scans) of the YSZ wafer (blue) and the MoS_2 layer (red), taken at $2\theta = 32.9°$ (MoS_2 10.0 Bragg reflection) and at $2\theta = 49.7°$ (YSZ $2\bar{2}0$ Bragg reflection). d) Epitaxial relationship scheme of YSZ wafer (marked in blue color) and MoS_2 layer (marked in red color).

© 2023 The Authors. physica status solidi (RRL) Rapid Research Letters published by Wiley-VCH GmbH

($\bar{2}$11) net-planes. This epitaxial relationship is outlined in Figure 1d. The in-plane lattice parameter $a_{exp} = 3.14$ Å derived from $2\theta/\phi$- scans, is very close to the literature value for bulk MoS_2, indicating that the layer is fully relaxed. Atomic force microscopy (AFM) images of the sample are shown Figure S2, Supporting Information.

Decreasing the layer thickness down to 1 ML is expected to result in the appearance of a photoluminescence (PL) band, corresponding to the transition from the indirect to direct band in the 2H-polytype of MoS_2.[14] **Figure 2**a displays reflection high-energy electron diffraction (RHEED) patterns from the bare YSZ wafer (top) and after deposition of about 0.5 ML-thick MoS_2 equivalent (bottom). The RHEED patterns show only one system of the streaky reflections from MoS_2 (shown by the blue lines with corresponding Miller indices in Figure 2a), indicating a 2D growth mode and a clear epitaxial relationship with the substrate (reflections of the YSZ substrate are highlighted by the red arrows) with sixfold symmetry, as previously verified for the multilayer sample. The relative distance between the MoS_2 streaks (blue lines) and the YSZ streaks (red lines) indicates that the MoS_2 layer is relaxed already in the first monolayer.

AFM image (Figure 2b) reveals MoS_2 islands with a lateral size of up to 100 nm. The islands are aligned along the step edges of the substrate, which have a miscut of about 0.4° toward the [1$\bar{3}$2] direction. The height of the islands of ≈0.7 nm is consistent with the thickness of a MoS_2 monolayer. The corresponding PL spectrum (Figure 2c) is composed of the PL band of MoS_2 (centered at 664 nm) with contributions of the YSZ wafer at 550 nm and 820 nm. It has to be noted that the tiny size of the crystallite domains, structural imperfection, and phase mixing during initial stages of the growth are the typical problems of PVD of TMDCs on non-van der Waals wafers.[15,16] For this reason, the well-ordered structure of MoS_2 nuclei, together with observation of the bright PL signal from the submonolayer thin film, represents a promising result, stimulating further process optimization.

The chemical and thermal stability of YSZ in the form of a thin and flexible ceramic substrate planarized with SiO_2 was recently demonstrated for CVD growth of few-layered MoS_2 films using ammonium heptamolybdate and sodium hydroxide as precursors.[17] In order to further prove the suitability of YSZ as a single-crystalline substrate for epitaxial growth of TMDCs, we performed a number of dedicated CVD growth experiments which are summarized in **Figure 3**. The layer orientation verified by RHEED coincides with that found in the PVD samples (Figure 3a). Optical microscopy reveals the formation of nonideal triangular MoS_2 domains with a size of 5–10 μm (Figure 3b). The single ML thickness and the 2H-phase of the domains are confirmed by PL measurements and AFM imaging. The PL spectrum of the sample shown in Figure 3c represents again a superposition of the signal from the layer and the substrate (red curve), while the measurements on the area in between the islands (black curve) depict the response of the substrate only. Optical microscopy clearly shows preferential in-plane epitaxial orientation of the islands. However, it is worth noting that antiparallel domains—that is, 180° domains—also show up. A closer

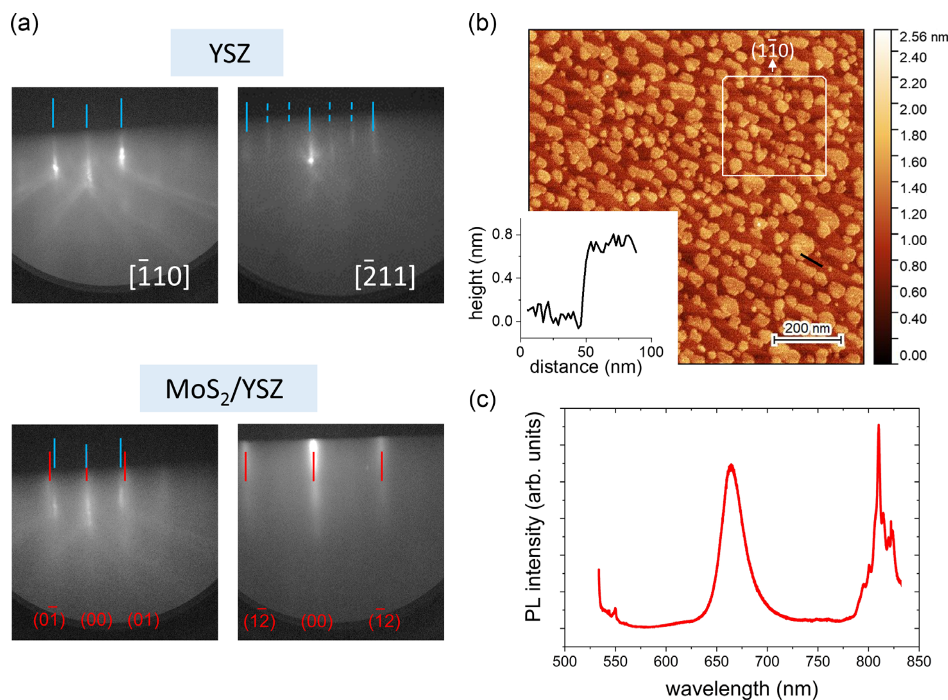

Figure 2. Submonolayer thin MoS_2 film grown by PVD on (111) YSZ. a) RHEED patterns of bare YSZ substrate (top, marked by blue lines) and MoS_2 layer deposited on YSZ (bottom, red lines). The dashed lines correspond to the surface reconstruction. The RHEED patterns were recorded along the [$\bar{1}$10] and [$\bar{2}$11] directions of the YSZ wafer. The Miller indices of the MoS_2 Bragg reflections (highlighted by red lines) are labeled. b) AFM image of the sample. The inset shows the in-plane orientation of the wafer and height profile along the black line. c) PL spectrum of the sample excited with a 532 nm laser line. The PL/Raman bands at 550 nm and 820 nm originate from the YSZ wafer.

© 2023 The Authors. physica status solidi (RRL) Rapid Research Letters published by Wiley-VCH GmbH

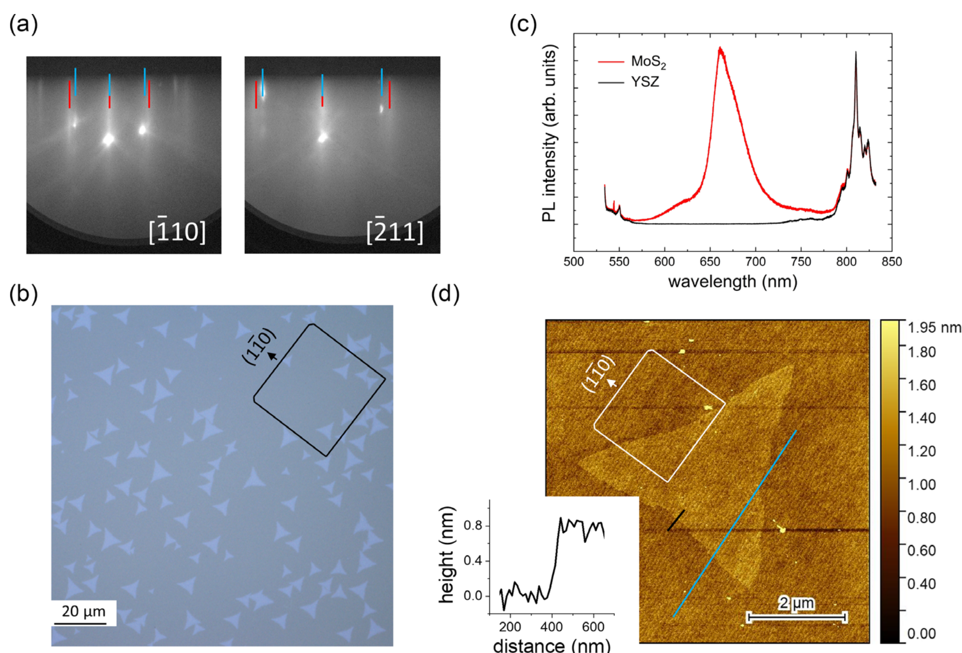

Figure 3. MoS_2 layer grown by CVD on YSZ (111) substrate. a) RHEED patterns of the sample recorded along the [$\bar{1}$10] and [$\bar{2}$11] directions of the YSZ wafer. Bragg reflections of the YSZ wafer and MoS_2 are highlighted by the red and blue lines, correspondingly. b) Optical micrograph, demonstrating in-plane preferential orientation of 1 ML-thick MoS_2 domains. c) PL spectra, from a MoS_2 island (red curve) and from the bare substrate surface (black curve). d) Overview AFM image of the triangular domain and the height profile along the black line. The blue line depicts the direction of atomic step edges of the wafer.

inspection of the sample by AFM reveals that one of the zigzag edges of the MoS_2 triangular is aligned perpendicular to the atomic steps of the wafer, appearing as a result of a substrate miscut of 0.2° toward the [1$\bar{1}$0] direction (Figure 3d). Statistical analysis of optical microscopy images (Figure S4, Supporting information) reveals that this alignment holds for 93% of the domains. The second observed variant corresponds to a 30° (or 90°) rotation of the MoS_2 crystals. The visual rotation of the crystallites can be attributed either to a transition from zigzag to armchain edges in about 7% of the domains or to a 90° rotation of MoS_2 lattice with respect to YSZ. In the latter case, the epitaxial supercell is formed by four MoS_2 units which commensurate with the substrate as $4 \times a_{\mathrm{MoS2}} \approx 2\sqrt{3} \times a_{YSZ\,110}$ with a lattice mismatch of about 0.3%. Despite the significantly smaller lattice mismatch compared to the in-plane alignment of MoS_2 (10$\bar{1}$0) || YSZ ($\bar{2}$11), the R30° variant appears to be energetically unfavorable, as it was rarely observed in the CVD samples and not detected in the PVD-grown films.

The results on PVD- and CVD-grown samples confirm that the in-plane epitaxial relationship between the MoS_2 layer and the YSZ substrate is not affected by the small random miscut direction of the wafer that results from wafer polishing. However, when depositing a material with threefold symmetry on a substrate with sixfold symmetry, it is expected from simple crystallographic considerations that 180° domains will be present in the layers. This can be clearly seen in the CVD-grown films. Note that both domain orientations are found with virtually equal incidence; however, these cannot be distinguished in our GIXD measurements. The identical scenario was recently reported for MoS_2 and WS_2 thin films deposited on c-plane sapphire. In that case, the degeneracy in the nucleation energies for parallel and antiparallel domains was successfully lifted by selecting a miscut orientation where the substrate step edges are aligned parallel to the zigzag edge of the triangular TMDC islands.[5,10] The observed similarity between sapphire and YSZ in terms of domain nucleation and growth process provides excellent perquisites for the fabrication of single-oriented TMDC layers on the substrate with smaller lattice mismatch. Careful design of the wafer miscut orientation in combination with appropriate growth stoichiometry plays an important role in this process.

3. Conclusion

We introduce Y-stabilized ZrO_2 (111) as a commonly available wafer for the epitaxial growth of TMDCs. The material has been found to be applicable for both PVD and CVD growth processes. MoS_2 layers grown on YSZ (111) with a small miscut toward the [1$\bar{3}$2] and [1$\bar{1}$0] directions exhibit sixfold symmetry and an in-plane epitaxial relationship with the wafer of (10$\bar{1}$0) MoS_2 || ($\bar{2}$11) YSZ according to GIXD and RHEED. Optical microscopy of the noncontinuous CVD layer reveals the presence of 180° rotation domains, as expected from epitaxial growth of a threefold material on a sixfold substrate. The observed similarity of the domain formation between sapphire and YSZ offers great opportunities for the fabrication of single-oriented TMDC layers on the substrate with smaller lattice mismatch by careful design of the wafer miscut orientation, combined with appropriate growth

© 2023 The Authors. physica status solidi (RRL) Rapid Research Letters published by Wiley-VCH GmbH

stoichiometry. The results are especially promising for the PVD process, where nucleation of MoS_2 islands with a lateral size of up to 100 nm and strong PL as expected for 2H-phase of MoS_2 in a single monolayer limit is observed already during the first growth runs.

4. Experimental Section

The epitaxial growth was performed on $10 \times 10 \times 0.5$ mm^3 YSZ (111) wafers (Crystec GmbH). The wafers were cleaned with organic solvents and annealed under air at 1000 °C for 2 h prior to the growth. In the case of PVD samples, a 500 nm-thick Mo layer was deposited on the back side of the substrate in order to improve the heat absorption and enable homogeneous heating of the sample. The growth temperature (T_G) was controlled by an infrared pyrometer with an emissivity factor of 0.7. The PVD samples were grown using pulsed thermal deposition technique.[18] A Mo wire with a diameter of 1.25 mm (GoodFellow, purity 99.9%) was used as a filament. Sulfur (S) was supplied by a valved cracker source (MBE Komponenten GmbH). The growth was performed via sublimating Mo in a pulsed mode under continuous exposure of the substrate to sulfur. The pulse duration and Mo sublimation period were set to 90 and 180 s, correspondingly. The sublimation current was adjusted to provide nominally single-ML equivalent Mo coverage during five pulses. The YSZ wafers were preheated prior to the growth under the S flux at 850 °C for 10 min. The deposition was performed at a growth temperature of $T_G = 620$ °C and S equivalent beam pressure of 3×10^{-7} Torr. The CVD sample was grown in a horizontal tube furnace with Ar carrier gas. MoO_3 powder was used as precursor. The CVD temperature was $T_{CVD} = 850$ °C. Raman and PL measurements were performed with a Horiba confocal Raman setup using a 532 nm laser line for the excitation and 1800 mm^{-1} optical grating. AFM was conducted with a Bruker Dimension in a ScanAsyst mode. The high-resolution X-ray diffraction experiments were performed on a 9 kW Rigaku SmartLab diffractometer. For the out-of-plane measurements, a parabolic multilayer mirror was used in combination with an asymmetric Ge 220 channel-cut crystal providing a monochromatic ($\lambda = 1.54056$ Å) and collimated (29 arcsec) X-ray beam. A Hypix 3000 2D area detector was used in 0D mode as a point detector. For the GIXD in-plane X-ray diffraction experiments, Soller slits were used for the in-plane collimation of the incident (0.15°) and diffracted (0.228°) beams. Typical glancing angles of incidence on the samples were below the critical angle of total external reflection to ensure maximum sensitivity to the MoS_2 film, typical value being 0.2°.

Supporting Information

Supporting Information is available from the Wiley Online Library or from the author.

Acknowledgements

The authors are grateful to IRIS Berlin Adlershof for the possibility of using experimental setups. The authors acknowledge financial support by the Deutsche Forschungsgemeinschaft (DFG) through the grants SA 3039/1-1 and Projektnummer 182087777-SFB 951. The authors thank European Regional Development Fund ERDF (project number 1.8/15) for funding this project.

Open Access funding enabled and organized by Projekt DEAL.

Conflict of Interest

The authors declare no conflict of interest.

Data Availability Statement

The data that support the findings of this study are available in the supplementary material of this article.

Keywords

MoS_2, transition metal dichalcogenides, YSZ, 2D materials

Received: April 13, 2023
Revised: May 30, 2023
Published online: June 25, 2023

[1] P. Ajaayn, P. Kim, K. Banerjee, *Phys. Today* **2016**, *69*, 38.
[2] I. Song, C. Park, H. C. Choi, *RSC Adv.* **2015**, *5*, 7495.
[3] B. Schönfeld, J. J. Huang, S. C. Moss, *Acta Cryst.* **1983**, *B39*, 404.
[4] N. Wakabayashi, H. G. Smith, R. M. Nicklow, *Phys. Rev. B* **1975**, *12*, 659.
[5] T. Li, W. Guo, L. Ma, W. Li, Z. Yu, Z. Han, S. Gao, L. Liu, D. Fan, Z. Wang, Y. Yang, W. Lin, Z. Luo, X. Chen, N. Dai, X. Tu, D. Pan, Y. Yao, P. Wang, Y. Nie, J. Wang, Y. Shi, X. Wang, *Nat. Nanotechnol.* **2021**, *16*, 1201.
[6] W. Mortelmans, S. E. Kazzi, B. Groven, A. N. Mehta, Y. Balaji, S. D. Gendt, M. Heyns, C. Merckling, *Appl. Phys. Lett.* **2020**, *117*, 033101.
[7] D. Dumcenco, D. Ovchinnikov, K. Marinov, P. Lazić, M. Gibertini, N. Marzari, O. L. Sanchez, Y.-Ch. Kung, D. Krasnozhon, M.-W. Chen, S. Bertolazzi, P. Gillet, A. Fontcuberta i Morral, A. Radenovic, A. Kis, *ACS Nano* **2015**, *9*, 4611.
[8] S. Wu, Ch Huang, G. Aivazian, J. S. Ross, D. H. Cobden, X. Xu, *ACS Nano* **2013**, *7*, 2768.
[9] W. Mortelmans, S. D. Gendt, M. Heyns, C. Merckling, *Appl. Mater. Today* **2021**, *22*, 100975.
[10] M. Chubarov, T. H. Choudhury, D. R. Hickey, S. Bachu, T. Zhang, A. Sebastian, A. Bansal, H. Zhu, N. Trainor, S. Das, M. Terrones, N. Alem, J. M. Redwing, *ASC Nano* **2021**, *15*, 2532.
[11] J. Wang, X. Xu, T. Cheng, L. Gu, R. Qiao, Z. Liang, D. Ding, P. Zheng, Z. Zhang, S. Zhang, G. Cui, C. Chang, C. Huang, J. Qi, J. Liang, C. Liu, Y. Zuo, G. Xue, X. Fang, J. Tian, M. Wu, Y. Guo, Z. Yao, Q. Jiao, L. Liu, P. Gao, Q. Li, R. Yang, G. Zhang, Z. Tang, et al., *Nat. Nanotechnol.* **2022**, *17*, 33.
[12] R. Wang, N. Koch, J. Martin, S. Sadofev, *Phys. Status Solidi RRL* **2023**, *17*, 2200476.
[13] A. Papadogianni, C. Wouters, R. Schewski, J. Feldl, J. Lähnemann, T. Nagata, E. Kluth, M. Feneberg, R. Goldhahn, M. Ramsteiner, M. Albrecht, O. Bierwagen, *Phys. Rev. Mat.* **2022**, *6*, 033604.
[14] K. F. Mak, Ch Lee, J. Hone, J. Shan, T. F. Heinz, *Phys. Rev. Lett.* **2010**, *105*, 136805.
[15] A. Barvat, N. Prakash, B. Satpati, S. S. Singha, G. Kumar, D. K. Singh, A. Dogra, S. P. Khanna, A. Singha, P. Pal, *J. Appl. Phys.* **2017**, *122*, 015304.
[16] Y. Wei, C. Hu, Y. Li, X. Hu, K. Yu, L. Sun, M. Hohage, L. Sun, *Nanotechnology* **2020**, *31*, 315710.
[17] Y. Zheng, Ch Yuan, S. Wei, H. Kim, F. Yao, J.-H. Seo, *Nanomaterials* **2019**, *9*, 1456.
[18] N. Mutz, T. Meisel, H. Kirmse, S. Park, N. Severin, J. P. Rabe, E. J. W. List-Kratochvil, N. Koch, C. T. Koch, S. Blumstengel, S. Sadofev, *Appl. Phys. Lett.* **2019**, *114*, 162101.

© 2023 The Authors. physica status solidi (RRL) Rapid Research Letters published by Wiley-VCH GmbH